Ocean Engineering 306 (2024) 118097

Contents lists available at ScienceDirect

Ocean Engineering

journal homepage: www.elsevier.com/locate/oceaneng

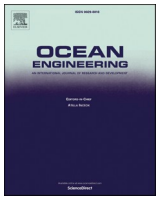

Research paper

# Trade-off between drag and catch performance when designing zooplankton trawls

Enis N. Kostak [a,*], Eduardo Grimaldo [a], Jesse Brinkhof [a], Bent Herrmann [a,b,c]

[a] UiT the Arctic University of Norway, Norwegian College of Fishery and Aquatic Science, Breivika, 9037, Tromsø, Norway
[b] SINTEF Ocean, Department of Fisheries Technology, 7010 Trondheim, Norway
[c] Technical University of Denmark, Section for Fisheries Technology, Institute for Aquatic Resources, 9850, Hirtshals, Denmark

ARTICLE INFO

*Keywords:*
Zooplankton harvesting
Net design optimization
Gear drag
Catch efficiency
*Calanus finmarchicus*

ABSTRACT

The aquaculture sector is in pursuit of sustainable and cost-effective raw materials for feed, and the copepod *Calanus finmarchicus* is a marine zooplankton species of commercial interest because of its high abundance in northern areas. These copepods have the potential to meet the demand for vast quantities of marine raw materials. However, the lack of an energy- and catch-efficient trawl technology has limited the development of this fishery. Therefore, this study investigated the effect of two central trawl net design parameters mesh size and taper angle to identify which values that provide optimal trade-off balance between gear drag and catch efficiency. We conducted flume tank experiments using a series of plankton nets varying in mesh size (250–1000 μm), solidity ratio (0.54–0.76), and taper angle (5°– 30°) to acquire data on gear drag. The same nets were then used in fishing trials to obtain data on their catch performance. This study shows that zooplankton nets with a mesh size of approximately 500 μm and a low taper angle of about 5° provided the best trade-off between drag and catch performance.

## 1. Introduction

Copepods (*Calanus* sp.), and especially *Calanus finmarchicus*, are a promising alternative marine resource with significant potential as a feed source for sustainable aquaculture. Distributed widely in the subarctic waters of the North Atlantic, *C. finmarchicus* dominates the zooplankton biomass across much of the coastal and deep North Atlantic Ocean (McBride et al., 2014). Recent estimates of between 200 and 400 million tons highlight the significant abundance of *Calanus* sp. (Aarflot et al., 2018). Based on data from a 0–200 m depth survey in May-June, –Skjoldal (2004) estimated that the Norwegian Sea contained 48.3 million tons of these copepods. Broms et al. (2016) reported an average biomass of 33 million tons wet weight and estimated that the annual production of *Calanus* sp. Can range between 193 and 290 million tons. Furthermore, *Calanus* sp. offers significant nutritional advantages. For example, the lipid content of *Calanus* sp. from northern Norwegian fjords can be as high as 70% of the dry weight; the lipid concentration peaks in summer and declines during the spawning season in late winter and early spring (Falk-Petersen et al., 1981).

The Norwegian Directorate of Fisheries has set an annual quota of 254,000 tons for the *C. finmarchicus* catch. However, despite its potential, the exploitation of *Calanus* sp. as a fishing resource is relatively low. Vessels with a limited *C. finmarchicus* trawl permit based on licensing regulations are authorized to harvest up to 3000 tons of *C. finmarchicus* in specific coastal areas per year. This permit allows harvesting of this species using a pelagic plankton trawl within Norway's Economic Zone and other defined regions (Norwegian Directorate of Fisheries, 2022). As the importance of sustainable aquaculture increases, the potential of *Calanus* sp. as a feed source is clear but requires development of sustainable harvesting technology.

Due to the small size *of C. finmarchicus* (3–4 mm), the fishery currently employs fine-meshed (low porosity) trawls with a mesh size of approximately 500 μm. The opening area of these trawls currently reach 120 $m^2$, with some vessels operating two such trawls simultaneously. The suitability of these trawls for large-scale zooplankton harvesting is debatable due to their high towing resistance (gear drag) and subsequent fuel consumption (Grimaldo and Gjøsund, 2012). The drag acting on these large trawls is influenced by several parameters, including mesh size, solidity ratio tapering angle and towing speed (Enerhaug, 2005; Gjøsund and Enerhaug, 2010; Grimaldo and Gjøsund, 2012; Grimaldo et al., 2023).

In the last two decades, driven by the interest of commercial

* Corresponding author.
*E-mail address:* enis.n.kostak@uit.no (E.N. Kostak).

https://doi.org/10.1016/j.oceaneng.2024.118097
Received 4 January 2024; Received in revised form 2 May 2024; Accepted 3 May 2024
Available online 10 May 2024

harvesting of zooplankton for food and feed industries, the knowledge obtained from studying small plankton sampling nets have been used to understand, design and optimise the performance of plankton trawls, which are much larger. The literature on the hydrodynamic performance of small plankton sampling nets is extensive and dates back to early 1960s. The filtration efficiency of such sampling nets has been studied through comprehensive experiments conducted in wind tunnels, flume tanks, and at sea (Tranter, 1967; Tranter and Heron, 1967; Breddermann, 2017). Likewise, the effect of design parameters on catch efficiency of plankton nets has also been assessed by several studies (Barnes and Tranter, 1965; Xiping et al., 2013). Evans and Sell (1985) evaluated the impact of mesh size on both catch and filtration efficiency for zooplankton sampling nets. Hernroth (1987) compared the performance of different plankton sampling nets particularly under high particle density conditions and emphasizes the influence of mesh size on sample composition. Additionally, the importance of mesh size in zooplankton sampling systems and its impact on catch efficiency for planktonic cnidarians in the equatorial Atlantic has been further explored (Skjoldal et al., 2013; Tosetto et al., 2019).

Further, based on flume tank experiments models that quantify the flow through and the forces acting on inclined nets provide expressions for the filtration efficiency and drag as functions design parameters such as twine diameter, mesh size, porosity, taper angle and flow (Gjøsund and Enerhaug, 2010; Grimaldo and Gjøsund, 2012). However, those models cannot be applied to complex trawl structures like tapering net sections and cylindrical codends.

Like for small plankton nets with low porosity, large commercial trawls that are specifically designed for harvesting *Calanus* sp., the filtration efficiency and towing resistance also strongly depends on the design parameters (mesh size, porosity, taper angle), operational conditions (towing speed, currents) and on the Reynolds number (Fridman, 1986), and may be significantly different for large low porosity commercial zooplankton trawls compared to more traditional high porosity fish trawls (Gjøsund and Enerhaug, 2010). The porosity of fish trawls is typically higher than 0.8, and the Reynolds number (based on twine thickness and knotted netting) is in the order of $10^3$-$10^4$. Consequently, the flow through the main part of traditional fish trawls is usually considered to be uniform and undisturbed by the trawl. Contrary to fish trawls, in trawls intended for commercial harvesting of *Calanus* sp., the mesh size and twine thickness are both in the order of $10^{-4}$ m, the porosity around 0.5, and the Reynolds number around $10^0$ -$10^2$ (Grimaldo and Gjøsund, 2012). Due to porosity, the entire flow field, filtered volume, and drag of such trawls depend strongly on the design parameters (twine thickness, mesh size, taper angle) and towing speed.

It is important to note that the requirements for energy and catch efficiency of small sampling plankton nets are not the same as for large commercial zooplankton trawls. Specifically, the operation of large low porosity commercial zooplankton trawls is highly energy demanding, compromising the sustainability of the fishery. Therefore, optimizing the value of design parameters and finding a trade-off that minimises the trawl drag while increasing the catch efficiency is sought.

To our knowledge, no study has been directly investigated the trade-off between reducing drag while maximizing catch efficiency of large low porosity trawls. Drag and catch efficiency are the two most important performance factors for sustainable *Calanus* sp. harvesting, and they both depend on the design parameters mesh size, solidity ratio, and taper angle. This study is therefore aimed at investigating the trade-off between reducing drag while maximizing catch efficiency. Therefore, the specific research questions this study is intended to answer are:

- To what extent do mesh size, solidity ratio, and taper angle of zooplankton nets affect gear drag?
- To what extent do mesh size, solidity ratio, and taper angle of zooplankton nets affect catch efficiency?
- Which mesh size and taper angle provide the best trade-off between drag and catch performance?

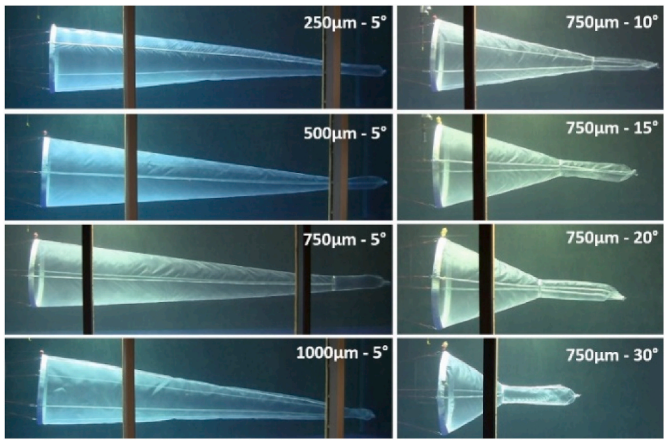


**Fig. 1.** Flume tank photos of all nets that were used in the study. Group 1 had different mesh sizes (left column), and group 2 had different taper angles (right column).

## 2. Materials and methods

We conducted flume tank experiments using a series of plankton nets varying in mesh size and taper angle to acquire data on gear drag. We used these data to establish predictive models for the effect of mesh size and taper angle on gear drag. Subsequently, we used the same nets in fishing trials to obtain data on catch efficiency. These data were used to establish predictive models for the effect of mesh size and taper angle on catch efficiency. Based on the predictive models of towing resistance and catch efficiency, we established a trade-off function as the ratio between catch efficiency and drag.

### 2.1. Experimental nets

To investigate the effect of different mesh sizes and taper angles on gear drag and catch efficiency, eight experimental plankton nets categorized into two main experimental groups based on their design parameters were used (Fig. 1). The first group consisted of four nets, each with a different nominal mesh size of 250, 500, 750, and 1000 µm (Fig. 1, left column), and a taper angle ($\alpha$) of 5°. The second group of nets had a mesh size of 750 µm and taper angles of 10°, 15°, 20°, or 30° (Fig. 1, right column).

All nets had the same principal design with identical mouth diameter ($d$) but varied in total length ($L$ + 95 cm), taper angle ($\alpha$), and mesh size (Fig. 2).

All experimental nets were square meshed and constructed of woven polyamide monofilament material, (Nylon PA 6.6). Each experimental net was attached to a plastic ring with 1 m diameter. The codend section, which had a diameter of 20 cm and a length of 95 cm, was sealed in the aft with a codline (Fig. 2). We measured mesh sizes using digital image analysis of netting samples, employing a Leica camera microscope (Wetzlar, Germany) for image acquisition and the FISHSELECT software (Herrmann et al., 2009) for the analysis. Bar lengths were measured vertically ($a$) and horizontally ($b$) from the middle of the bars, along with twine diameter ($t$) (Appendix Fig. A1). Ten individual meshes were measured from each netting sample. The measured mesh size ($w$) for each sample was calculated as the mean of the 10 $a$ and $b$ measurements ($(a + b)/2$) (Table 1).

The microscope images were also used to calculate the solidity ratio ($s$) for each mesh size net using the ImageJ software tool. Binary images were generated to determine the solidity ratio by quantifying the area of the netting structure (represented by the number of pixels in the netting) and then dividing the area by the total area projected in the image. The solidity ratio varied between 0.5410 and 0.7650 for the tested mesh sizes (Table 1).

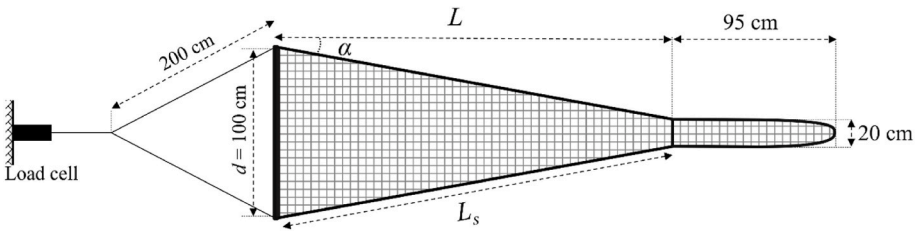


**Fig. 2.** Plankton net design and experimental setup in flume tank $L$: conus length, $L_S$: side conus length, $d$: mouth diameter, $\alpha$: taper angle.

**Table 1**
Geometric properties of the eight nets tested (Figs. 1 and 2). $w$: measured mesh size, $\alpha$: taper angle, $L$: conus length, $L_S$: side conus length, $a$: vertically measured bar length, $b$: horizontally measured bar length, $t$: twine thickness, $s$: solidity. Standard deviations are in parentheses.

| Net Name | 5 × 250 | 5 × 500 | 5 × 750 | 5 × 1000 | 10 × 750 | 15 × 750 | 20 × 750 | 30 × 750 |
|---|---|---|---|---|---|---|---|---|
| Nominal Mesh size [μm] | 250 | 500 | 750 | 1000 | 750 | 750 | 750 | 750 |
| $w$ [μm] | 194 (7.75) | 446 (13.29) | 655.5 (7.98) | 898.5 (16.17) | 655.5 (7.98) | 655.5 (7.98) | 655.5 (7.98) | 655.5 (7.98) |
| $\alpha$ [°] | 5 | 5 | 5 | 5 | 10 | 15 | 20 | 30 |
| $L$ [cm] | 438 | 438 | 438 | 438 | 223 | 140 | 114 | 67 |
| $L_s$ [cm] | 440 | 440 | 440 | 440 | 227 | 146 | 120 | 78 |
| $a$ [μm] | 187 (11.59) | 431 (23.31) | 676 (15.06) | 929 (17.29) | 676 (15.06) | 676 (15.06) | 676 (15.06) | 676 (15.06) |
| $b$ [μm] | 201 (7.38) | 461 (13.7) | 635 (8.50) | 868 (27.41) | 635 (8.50) | 635 (8.50) | 635 (8.50) | 635 (8.50) |
| $t$ [μm] | 198 (10.33) | 345 (20.68) | 318 (16.87) | 514 (12.65) | 318 (16.87) | 318 (16.87) | 318 (16.87) | 318 (16.87) |
| $s$ | 0.7650 | 0.6624 | 0.5410 | 0.5700 | 0.5410 | 0.5410 | 0.5410 | 0.5410 |

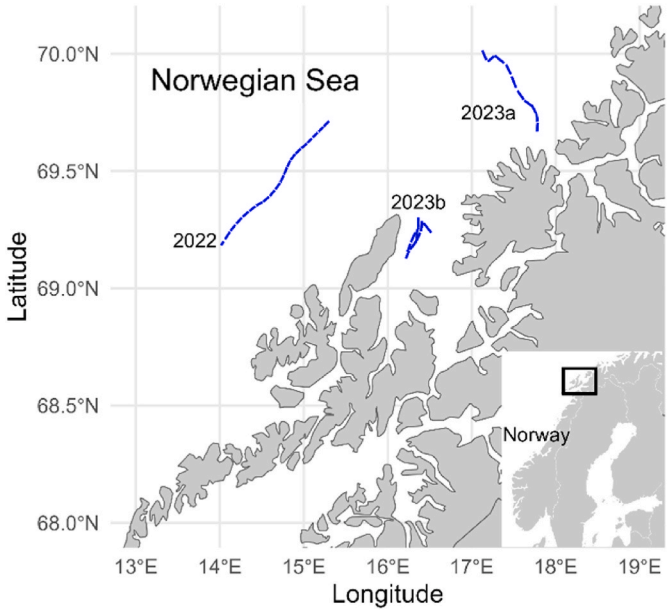


**Fig. 3.** Study area and towing lines for the years 2022 and 2023 (a, b).


**Fig. 4.** Experimental setup used during the cruise in 2022 with towing frames with different mesh size (top left) and taper angle (top right). Experimental setup for the cruise in 2023 (bottom).

### 2.2. Flume tank experiments

Flume tank experiments were aimed at assessing the drag forces of the nets. The flume tank experiments were conducted in June 2022 at the North Sea A/S flume tank located in Hirtshals, Denmark. The flume tank measured 21.3 m in length, 8.0 m in width, and 2.7 m in depth, with a total volume of ~460 $m^3$ of fresh water. Maximum water speed in this tank was 1 m/s.

For the drag measurements, a net was attached to a towing wire, which was connected to the load cells (Fig. 2). This wire was stabilized by four evenly spaced 2 m long bridles, each anchored to the net's hoop. The bridles converged into a single towing wire to centralize the force exerted on the load cells. To enhance stability and minimize oscillatory movements during towing, the wire passed through a smaller ring, which was fastened to the tank walls on both sides, ensuring a controlled and steady motion for accurate drag readings.

Drag data were obtained from two submersible miniature S-beam load cells (Model LSB210 FUTEK, Irvine, CA, USA) mounted between the tank wall and the towing wire, which had a capacity of 445 N. The accuracy of these load cells was within 0.2% of the rated output. Each load cell was individually connected to a dedicated hardware channel, allowing for simultaneous and synchronized data gain every 0.02 s (50

Hz sampling rate). For the gear drag, over 15,000 readings were collected for each net. Each net was individually tested in the tank with water speeds at 0.31, 0.51, 0.72, and 0.98 m/s. The tests were repeated five times for each net with each speed. The same flume tank tests were used to study the effect of gear design parameters on filtration efficiency (Grimaldo et al., 2023).

### 2.3. Fishing trials

Fishing trials were aimed at assessing the catch efficiency of the nets. The sea trials were conducted onboard the R/V "Helmer Hanssen" (63.8 m LOA, 4080 HP) during two cruises. The first cruise was carried out on June 15–16, 2022 in the Norwegian Sea between 69°06′–69°24′N and 14°00′–15°08′E along the continental shelf across Langøya and Andøya Islands in Northern Norway. The second cruise occurred the following summer from June 10 to 13, 2023 and covered two different towing areas labelled as 2023a (69°24′N–70°00′N and 17°27′E–17°04′E) and 2023b (69°10′N–69°08′N and 16°13′E–16°18′E) (Fig. 3). The towing duration was 60 min in 2022 and 120 min in 2023. The average towing speed was 1.97 knots (ranging from 1.1 to 2.6 knots, or 0.57–1.34 m/s), and the average towing depth was 7.3 m (ranging from 13.8 m to 2.5 m).

The same nets used in the flume tank were used during the fishing trials to assess their catch efficiency. The nets were mounted in two steel frames (2.1 × 2.1 m). One frame was equipped with the four nets with different mesh sizes, and the other frame was equipped with the four nets with different taper angles (Fig. 4). Four plastic (~23 cm) floats were tied to the top of each frame, and a chain weight was attached to the bottom of the frame to maintain a perpendicular towing position. A Scanmar SS4 depth sensor (Åsgårdstrand, Norway) was attached in the middle of the upper bar of the frame to control the towing depth.

During the trials in 2022, each frame was fished one at a time, alternating between them; in 2023, the two frames were welded together and fished simultaneously (Fig. 4). The advantages of fishing the nets simultaneously in the quattro-setup (as during the cruise in 2022) and in the octa-setup (as during 2023) was that the nets are exposed to the same varying fishing conditions, which increased the power of the analysis of their relative fishing performances (Cerbule et al., 2023).

After each tow, the catch from each net was emptied into separate containers, and the weight of each catch was measured on a scale with a precision of 0.001 kg.

### 2.4. Assessment of drag and catch ratio

Drag results from flume tank experiments and catch data from fishing trials were used to assess the effect of net design on drag and catch efficiency. To make our results as extrapolative as possible and to obtain the best signal-to-noise ratio as possible, the nets were exposed to exactly the same experimental conditions, and their performance was quantified in terms of ratios. The advantage of this approach was that the results from the net comparisons were less sensitive to the specific conditions during the experimental trials (Frandsen et al., 2011). Therefore, results obtained for net drag ($D$) (section 2.2) and net catch ($C$) (section 2.3) were transformed to drag ratio ($DR$) and catch ratio ($CR$) (in %) before further analysis as follows:

$$DR_i = 100 \times \frac{\sum_{j=1}^{n} D_{ij}}{\sum_{j=1}^{n} D_{bj}}$$
$$CR_i = 100 \times \frac{\sum_{j=1}^{n} C_{ij}}{\sum_{j=1}^{n} C_{bj}} \quad (1)$$

where $DR_i$ is the $DR$ for net designs $i \in \{5\times250, 5\times500, 5\times750, 5\times1000\}$ for design group 1 and $i \in \{5\times750, 10\times750, 15\times750, 30\times750\}$ for design group 2. $DR_i$ quantifies the drag for this design relative to the drag of one of the other designs. The $b$ was chosen as the baseline to which the others were compared. The $n$ is the number of repeated measurements in the flume tank experiments (section 2.2). $CR_i$ is the $CR$ for net design $i$ that quantifies the catch for this design relative to the catch of one of the other designs, $b$ was chosen as the baseline to which the others were compared, and $n$ is number of hauls during the fishing experiments (section 2.3). The baseline used in group 1 (different mesh sizes) was $b = 5 \times 750$, and in group 2 (different taper angles) it was $b = 10 \times 750$ (Table 1). Thus, estimations were carried out separately for design group 1 and 2 for evaluating the effect of mesh size and taper angle, respectively.

Uncertainties in the form of Efron 95% percentile confidence intervals (CIs) (Efron, 1982) for $DR_i$ and $CR_i$ were obtained using the bootstrap method by resampling $n$ measurements/hauls using 1000 repetitions. The analysis of $DR_i$ and $CR_i$ were conducted using the statistical analysis tool SELNET (Herrmann et al., 2012, 2022).

### 2.5. Models for effect of mesh size and taper angle on drag and catch ratio

To model the effect of mesh size and taper angle on drag and catch ratio we considered the following empirical models:

$$r(p) = \begin{cases} M1: & a \times p \\ M2: & a \times p + b \\ M3: & \frac{a}{sin(p)} \\ M4: & \frac{a}{sin(p)} + b \\ M5: & \frac{a}{tan(p)} \\ M6: & \frac{a}{tan(p)} + b \\ M7: & \frac{a}{1.0 + exp(b \times (p - c))} \end{cases} \quad (2)$$

where the response variable $r(p)$ was set to drag ratio ($DR$) and catch ratio ($CR$) one at time, and the input parameter to $w$ and $\alpha$ depending on if it was group 1 (nets with different mesh sizes) or group 2 (nets with different taper angles) being analysed. For the analysis of the $DR$ results, models M1 to M7 in equation (2) were applied separately for each water speed tested in the flume tank. However, the drag of a net is only indirectly correlated to mesh size through the net solidity (Zhou et al., 2015). Therefore, when modelling the effect of mesh size on $DR$, the input variable $p$ was first assigned to the value of the solidity of the net ($s$) and then after the modelling $s$ was substituted by equation (3) (see Appendix) to obtain a description of how $DR$ depends on mesh size $w$:

$$s = \frac{t \times (t + 2 \times w)}{t \times (t + 2 \times w) + w^2} \quad (3)$$

Using equation (3), $DR(s)$ leads to $DR(w,t)$, implying that net twine thickness needed to be considered when substituting $s$ with its relation to $w$.

The models M1 and M2 in equation (2) were linear models for the response as a function of the input variable. Models M3 to M6 included trigonometric functions $\sin(p)$ or $\tan(p)$ and were based on the premise that the total area or volume inside the net might drive the value of the response variable. These models could therefore be particularly relevant

**Table 2**
Mean drag in newtons [N] for the tested nominal mesh sizes and taper angles for each water speed [m/s]. Values in parentheses represent 95% CIs.

| Net design | 0.31 [m/s] | 0.51 [m/s] | 0.72 [m/s] | 0.98 [m/s] |
|---|---|---|---|---|
| 5 × 250 | 64.3 (64.2–64.5) | 172.4 (171.4–172.9) | 335.2 (332.6–337.8) | 617.4 (611.7–623.2) |
| 5 × 500 | 57.8 (57.7–57.9) | 157.5 (156.6–157.9) | 311.5 (307.8–314.3) | 577.4 (573.8–581.0) |
| 5 × 750 | 49.4 (48.8–49.7) | 133.9 (133.7–134.0) | 266.6 (262.8–270.1) | 505.1 (496.5–510.3) |
| 5 × 1000 | 50.9 (50.8–51.3) | 140.2 (139.1–141.2) | 276.9 (272.7–280.1) | 521.6 (517.1–526.5) |
| 10 × 750 | 41.7 (41.4–42) | 110.3 (109.3–110.9) | 216.1 (211.9–220.2) | 406.8 (404.5–409.2) |
| 15 × 750 | 39 (38.6–39.3) | 101.8 (101.4–102.1 | 193.0 (191.4–194.4) | 354.3 (352.9–355.9) |
| 20 × 750 | 37.4 (36.9–37.8) | 97.2 (96.7–97.6) | 184.9 (182.9–186.4) | 332.5 (331.1–333.8) |
| 30 × 750 | 37.5 (37.1–37.8) | 98.6 (98.3–99.0) | 187.2 (185.0–188.6) | 336.2 (335.0–337.7) |

when $p = \alpha$. Model M7 provided an S-shaped (sigmoidal) response as a function of the input parameter and could be particularly relevant when modelling *CR* catch.

The model selection was based on the Akaike information criterion (AIC) value for each response *DR* and *CR* with each input parameter *w* and α separately (Akaike, 1974), and the model with the lowest value was chosen. For the selected model in each case, the $R^2$ value was used to quantify the ability of the model to describe the trend in the data. The analysis was conducted using R Studio (version 2022.07.11), with functions *lm()* and *nls()* applied to fit the models in equation (2) to the data. For graphical output, we used R package *ggplot2*.

### 2.6. Trade-off between catch and drag performance

Based on the predictive models for effect of mesh size and taper angle on *DR* and *CR*, respectively, we established trade-off (*TR*) functions. The two trade-off functions, one for effect of mesh size and the other for taper angle, were quantified as the ratio between *CR* and *DR*:

$$\begin{aligned} TR(w,t) &= CR(w)/DR(w,t) \\ TR(\alpha) &= CR(\alpha)/DR(\alpha) \end{aligned} \quad (4)$$

A higher value of the trade-off functions was better. Thus, equation (4) was used to identify which mesh size and taper angle provided the best trade-off between catch performance (as high as possible) and drag performance (as low as possible).

## 3. Results

### 3.1. Drag ratio as a function of solidity, mesh size, and taper angle

Table 2 presents the results for drag measurements for the nets tested in the flume tank at different water speeds. We transformed the mean drag forces presented in Table 2 to drag ratios by applying equation (1) (Table 3).

Models to quantify the drag ratio as a function of net solidity were obtained by applying equation (2) to the drag ratio data presented in Table 3 together with the net solidity data for different designs (Table 1). This process was conducted for each of the four water speeds tested in the flume tank. In general, model M2 (equation (2)) performed best for all water speeds (*U*), as it had the lowest AIC values among the models tested (Table 4). Therefore, M2 was selected as the model for all water speeds, and the results showed that the drag ratio increased linearly with increasing solidity (Fig. 5). $R^2$ values were 0.9986, 0.9942, 0.9865, and 0.9889 for the water speeds 0.31, 0.51, 0.72, and 0.98 m/s, respectively, which demonstrated that the model represented the trends in the experimental data well.

Inserting the mesh sizes and twine thicknesses for the individual nets (Table 1) into equation (3) and using the resulting solidity values as input into the model established for *DR(s)* enabled us to visualise our *DR* model predictions versus mesh size and compare the model predictions with the experimentally obtained data points from the flume tank (Fig. 6).

The predicted values for drag ratio versus mesh size for the nets tested showed high agreement with the experimentally obtained data for all nets at all water speeds (Fig. 6), which demonstrated the validity of our approach. Therefore, we used this method to quantify how the drag ratio depended on mesh size and twine thickness (Fig. 7).

Our results showed that to maintain the same drag ratio if reducing the mesh size, the twine thickness needed to be reduced (Fig. 7). This was also clear from the correlation between net solidity, mesh size, and twine thickness as presented by equation (3) combined with the fact that the drag ratio was well modelled as a single parameter function of the net solidity, as demonstrated by the high $R^2$ values obtained (see above).

Considering the drag ratios for different taper angles, model M4 had the lowest AIC values for the water speeds tested (Table 4). For this model, the corresponding $R^2$ values were 0.9905, 0.9830, 0.9823, and 0.9825 for water speeds of 0.31, 0.51, 0.72, and 0.98 m/s, respectively (Fig. 8). This demonstrated the ability of the model to describe the main

**Table 4**
AIC values for the models tested on the drag ratios (*DR*) versus net solidity (*s*) and taper angle (*α*) for each water speed tested (*U*). Models with the lowest AIC are in bold.

| | Model | 0.31 [m/s] | 0.51 [m/s] | 0.72 [m/s] | 0.98 [m/s] |
|---|---|---|---|---|---|
| *DR(s)* | M1 | 47.88 | 47.77 | 47.59 | 47.32 |
| | M2 | **30.37** | **30.66** | **29.68** | **28.47** |
| | M3 | 52.53 | 52.50 | 52.40 | 52.26 |
| | M4 | 36.14 | 35.79 | 34.95 | 33.77 |
| | M5 | 52.51 | 52.48 | 52.38 | 52.23 |
| | M6 | 35.97 | 35.63 | 34.78 | 33.60 |
| | M7 | 55.57 | 55.62 | 51.72 | 51.72 |
| *DR(α)* | M1 | 58.20 | 58.38 | 58.55 | 58.69 |
| | M2 | 38.27 | 40.15 | 41.44 | 42.00 |
| | M3 | 56.15 | 55.86 | 55.32 | 54.71 |
| | M4 | **20.53** | **24.88** | **26.54** | **27.63** |
| | M5 | 56.57 | 56.30 | 55.76 | 55.20 |
| | M6 | 21.38 | 25.58 | 27.14 | 27.96 |
| | M7 | 47.90 | 66.63 | 50.70 | 65.93 |

**Table 3**
Drag ratio (*DR*) values for all nets and water speeds tested, with CIs in parentheses.

| Net design | 0.31 [m/s] | 0.51 [m/s] | 0.72 [m/s] | 0.98 [m/s] |
|---|---|---|---|---|
| 5 × 250 | 130.37 (129.9–131.4) | 128.78 (128.2–129.0) | 125.69 (125.1–126.6) | 122.24 (122.1–123.2) |
| 5 × 500 | 117.22 (116.6–118.2) | 117.66 (117.2–117.9) | 116.82 (116.4–117.2) | 114.32 (113.9–115.6) |
| 5 × 750 | 100 | 100 | 100 | 100 |
| 5 × 1000 | 103.33 (103.2–104.0) | 104.77 (104.1–105.3) | 103.83 (103.7–103.8) | 103.28 (103.2–104.2) |
| 10 × 750 | 84.45 (84.5–84.7) | 82.38 (81.7–82.8) | 81.04 (80.6–81.5) | 80.54 (80.2–81.5) |
| 15 × 750 | 79.12 (79.0–79.2) | 76.03 (75.8–76.2) | 72.36 (71.9–72.9) | 70.14 (69.7–71.1) |
| 20 × 750 | 75.71 (75.6–76.1) | 72.61 (72.3–72.8) | 69.32 (69.0–69.6) | 65.83 (65.4–66.7) |
| 30 × 750 | 75.94 (75.1–76.1) | 73.69 (73.5–73.9) | 70.20 (69.8–70.4) | 66.57 (66.2–67.5) |

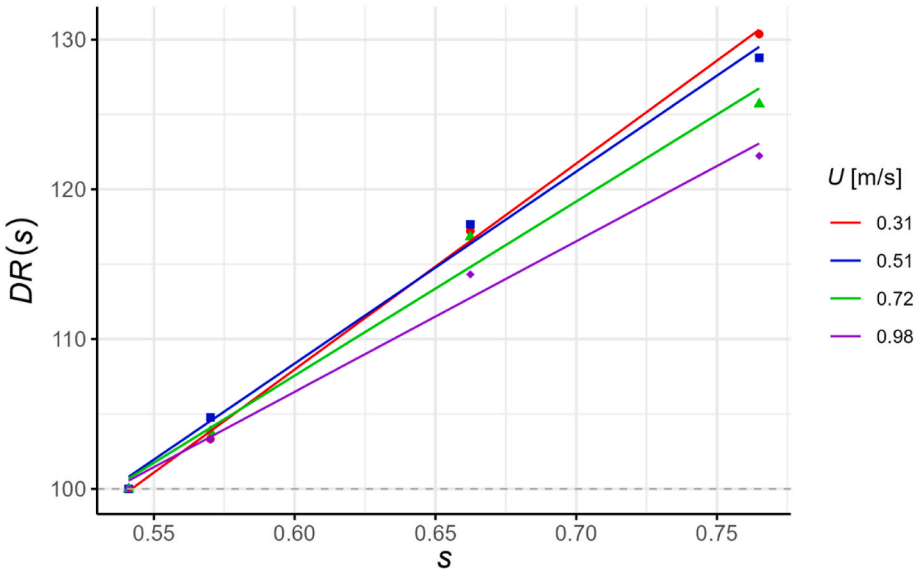


**Fig. 5.** Drag ratio (*DR*) in relation to solidity (*s*) for each water speed (*U*) tested.

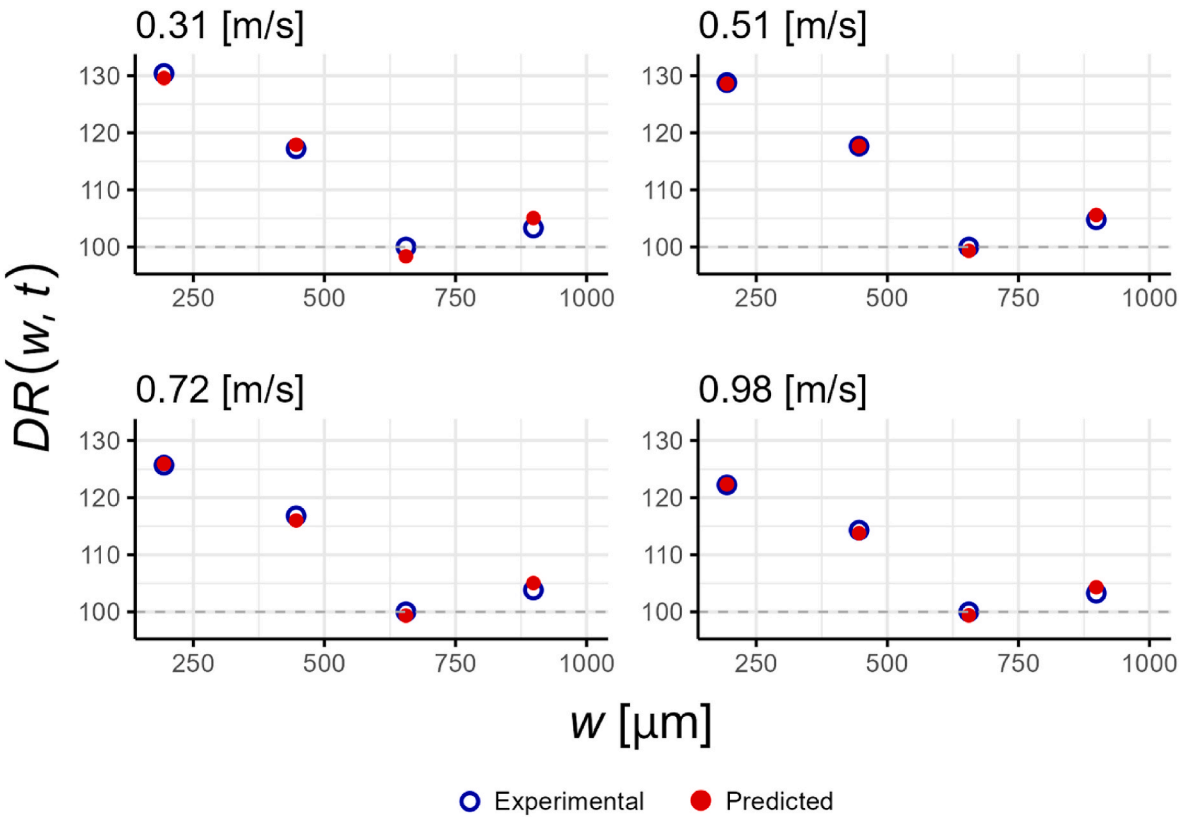


**Fig. 6.** Drag ratio (*DR*) versus mesh size (*w*).

trends in the experimental data.

In general *DR(α)* demonstrated a decrease in drag as the taper angle increased (Fig. 8). The rate of decrease in the drag ratio is highest for the lower taper angles. Additionally, increased water speed corresponded to an increase in the *DR*.

### 3.2. Catch ratio in relation to mesh size and taper angle

During the cruise in 2022, we conducted 10 hauls using each quattro-set-up, while in 2023 we conducted 22 hauls with the octa-set-up. Catch weights varied among individual nets due to varying catch densities (Fig. 9). During both cruises, catches where generally very clean and consisted entirely of small-sized species dominated by *C. finmarchicus* (see supplementary material).

The catch weights presented in Fig. 9, were transformed to catch ratios (*CR*) following equation (1) (Table 5). Fitting the models in equation (2) to the catch ratio values presented in Table 5 showed that model M7 had the lowest AIC for the group of nets with different mesh sizes (Table 6). For the nets with different taper angles, M6 had the lowest AIC value for the trials in 2022, whereas model M5 had the

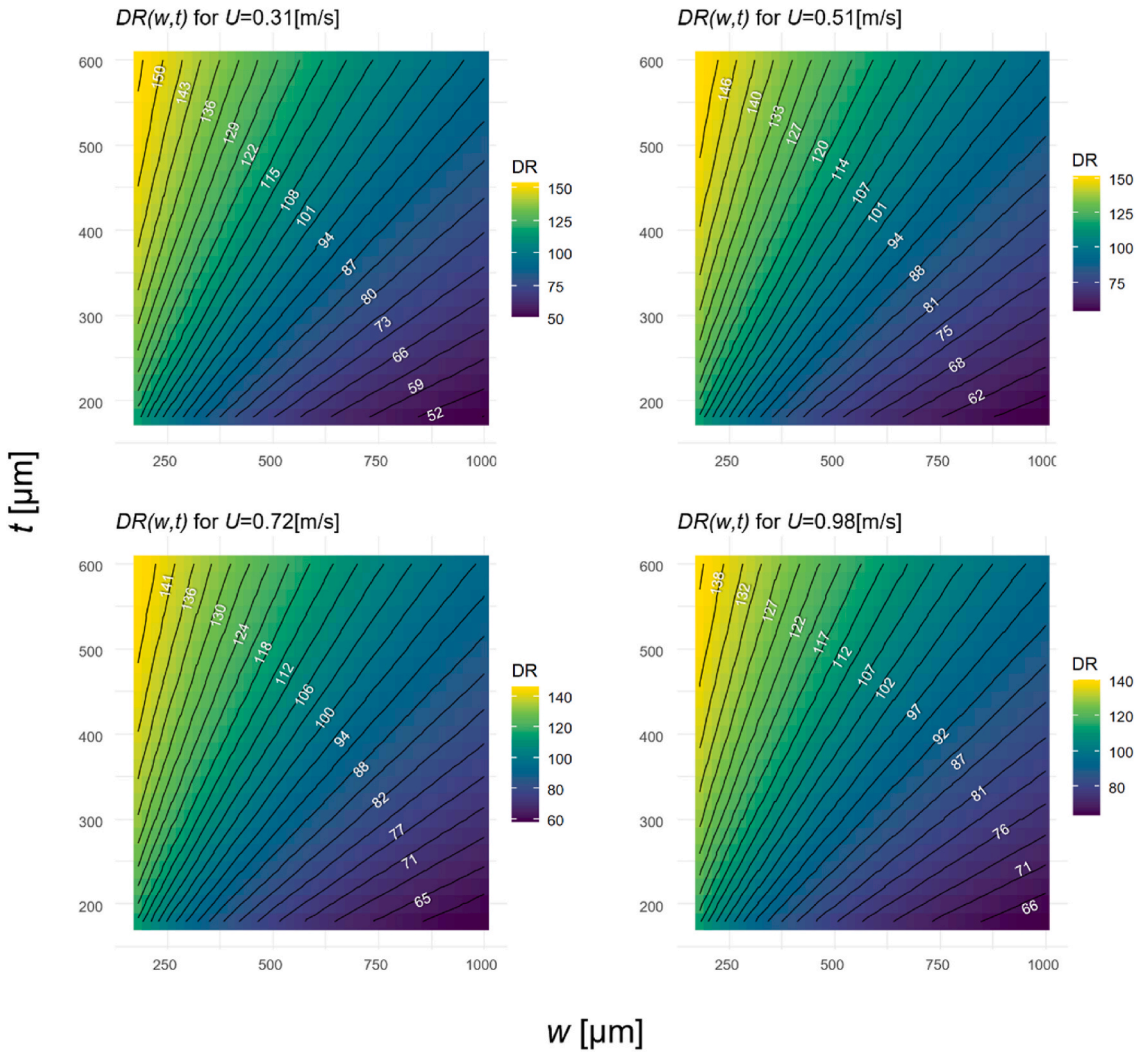


**Fig. 7.** Iso-plots for drag ratio (*DR*) versus mesh size (*w*) and twine diameter (*t*) for different water speeds.

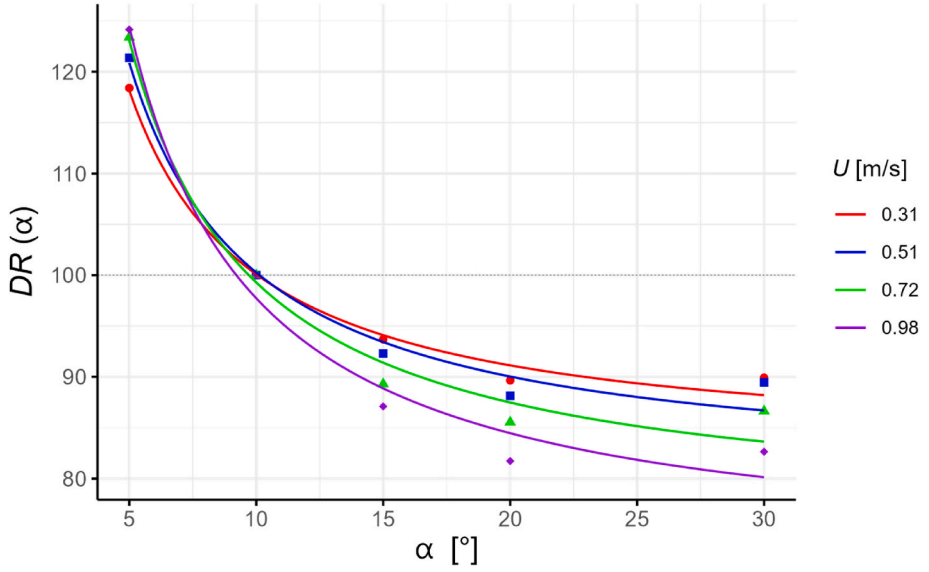


**Fig. 8.** Drag ratio (*DR*) against taper angle ($\alpha$) at different water speeds (*U*).

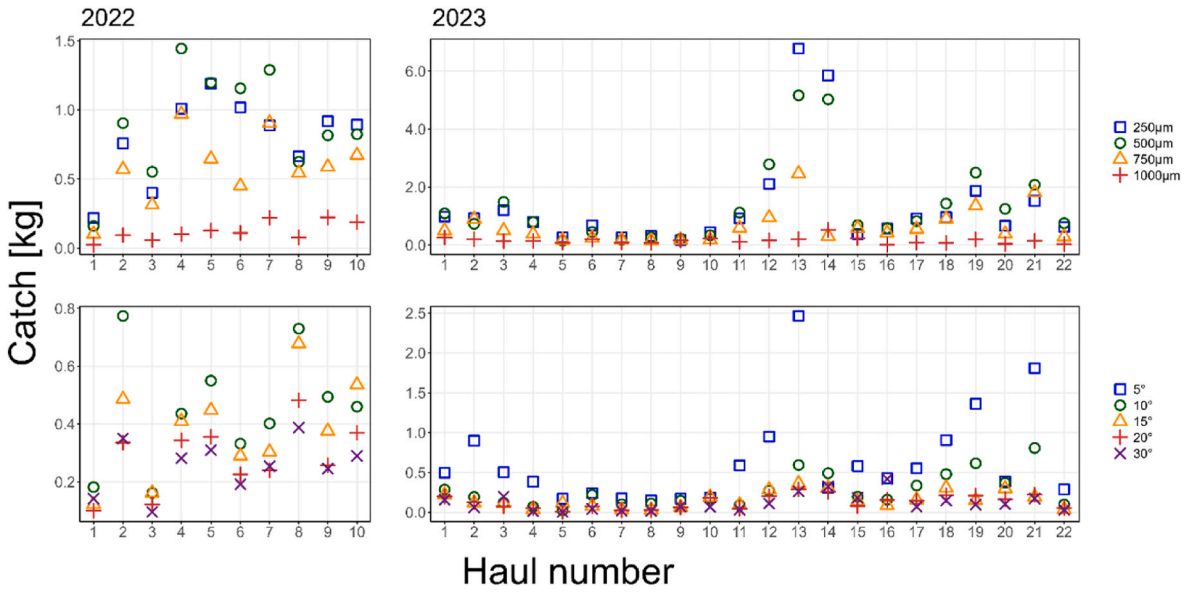


**Fig. 9.** Catch [kg] across all hauls for the nets with different mesh size (top left; 2022, top right; 2023). Catch weight per haul for nets with different taper angle in year 2022 (bottom left) and 2023 (bottom right).

**Table 5**
Catch ratio (*CR*) values for all tested nets with different mesh sizes (*w*) and taper angles ($\alpha$). Values in parentheses represent 95% CIs.

| | Net design | 2022 | 2023 |
|---|---|---|---|
| *CR(w)* | 5 × 250 | 138.08 (116.6–164.7) | 208.46 (135.4–319.1) |
| | 5 × 500 | 155.61 (137.5–180.7) | 213.42 (155.7–308.6) |
| | 5 × 750 | 100 | 100 |
| | 5 × 1000 | 21.24 (16.0–26.6) | 24.31 (16.2–38.3) |
| *CR(α)* | 5 × 750 | – | 234.68 (179.8–295.9) |
| | 10 × 750 | 100 | 100 |
| | 15 × 750 | 84.30 (73.5–94.4) | 57.85 (45.7–73.9) |
| | 20 × 750 | 62.67 (54.2–78.8) | 48.41 (40.5–58.1) |
| | 30 × 750 | 56.40 (51.3–62.3) | 44.21 (30.6–64.9) |

**Table 6**
AIC values for modelled catch ratio (*CR*) versus mesh size (*w*) and taper angle ($\alpha$) for both years.

| | Model | 2022 | 2023 |
|---|---|---|---|
| *CR(w)* | M1 | 51.24 | 54.19 |
| | M2 | 43.25 | 44.23 |
| | M3 | 53.37 | 55.84 |
| | M4 | 41.97 | 47.88 |
| | M5 | 53.37 | 55.84 |
| | M6 | 40.96 | 47.24 |
| | M7 | **36.39** | **38.29** |
| *CR(α)* | M1 | 45.50 | 56.23 |
| | M2 | 32.13 | 49.53 |
| | M3 | 35.13 | 34.18 |
| | M4 | 27.88 | 34.07 |
| | M5 | 36.54 | **33.65** |
| | M6 | **27.81** | 34.90 |
| | M7 | 44.19 | 61.01 |

lowest AIC for the year 2023 (Table 6).

For model M7, which was applied to mesh size (*w*), the corresponding $R^2$ values were 0.9734 for 2022 and 0.9818 for 2023 (Fig. 10). These values demonstrated the ability of the model to describe the main trends in the experimental data. For mesh sizes up to 500 µm, the catch ratio only decreased slightly, but mesh sizes >500 µm showed a significant decrease in the catch ratio (Fig. 10).

For model M6, which was applied to nets with different taper angle from the trials in 2022, the corresponding $R^2$ value was 0.9547. For the year 2023, model M5 was applied as the best model, and it had an $R^2$ value of 0.9763. These results showed that catch ratio decreased as taper angle increased (Fig. 8). The rate of decrease was highest for the smallest taper angles.

### 3.3. Trade-off between catch ratio and drag ratio

Based on the models established for catch and drag ratio, trade-off functions were created following equation (4) for mesh size (*w*) and taper angle ($\alpha$) (Fig. 11). For both *DR(w,t)* and *DR(α)*, the results were specifically chosen for the water speed of 0.98 m/s, as this speed represented most closely the average towing speed used during the sea trials.

The mesh size trade-off function showed that the optimal mesh size was be around 500 µm (Fig. 11). Reducing mesh size would require a simultaneous reduction of twine thickness to avoid obtaining a lower and less favourable trade-off score. The taper angle trade-off function demonstrated that a very small taper angle was most favourable, as the highest taper angle provided the poorest trade-off value despite being the lightest design to tow (Figs. 9 and 11).

## 4. Discussion

This study investigated the trade-off between reducing hydrodynamic drag while maximizing catch efficiency of low porosity trawls intended for commercial harvesting of zooplankton. First, we conducted drag measurements in a flume tank with low porosity nets and provided expressions for the drag as functions of mesh size, porosity, taper angle, and water speed. Our results showed that the drag of the square-meshed conical nets increased with increasing velocity and solidity. Drag also increased with increasing netting taper angle to the flow. The fact that the drag increases with the towing speed, is crucial for the fuel efficiency of larger commercial zooplankton trawls. Our flume tank experiments confirmed the influence of mesh size, solidity ratio and tapering angle on the resulting drag of the nets. Second, we applied the same nets in fishing trials to assess the catch performance. Third, combining the results from the flume tank and fishing trials enabled us to establish functions for the trade-off balance between gear drag and catch efficiency dependent on mesh size and taper angle.

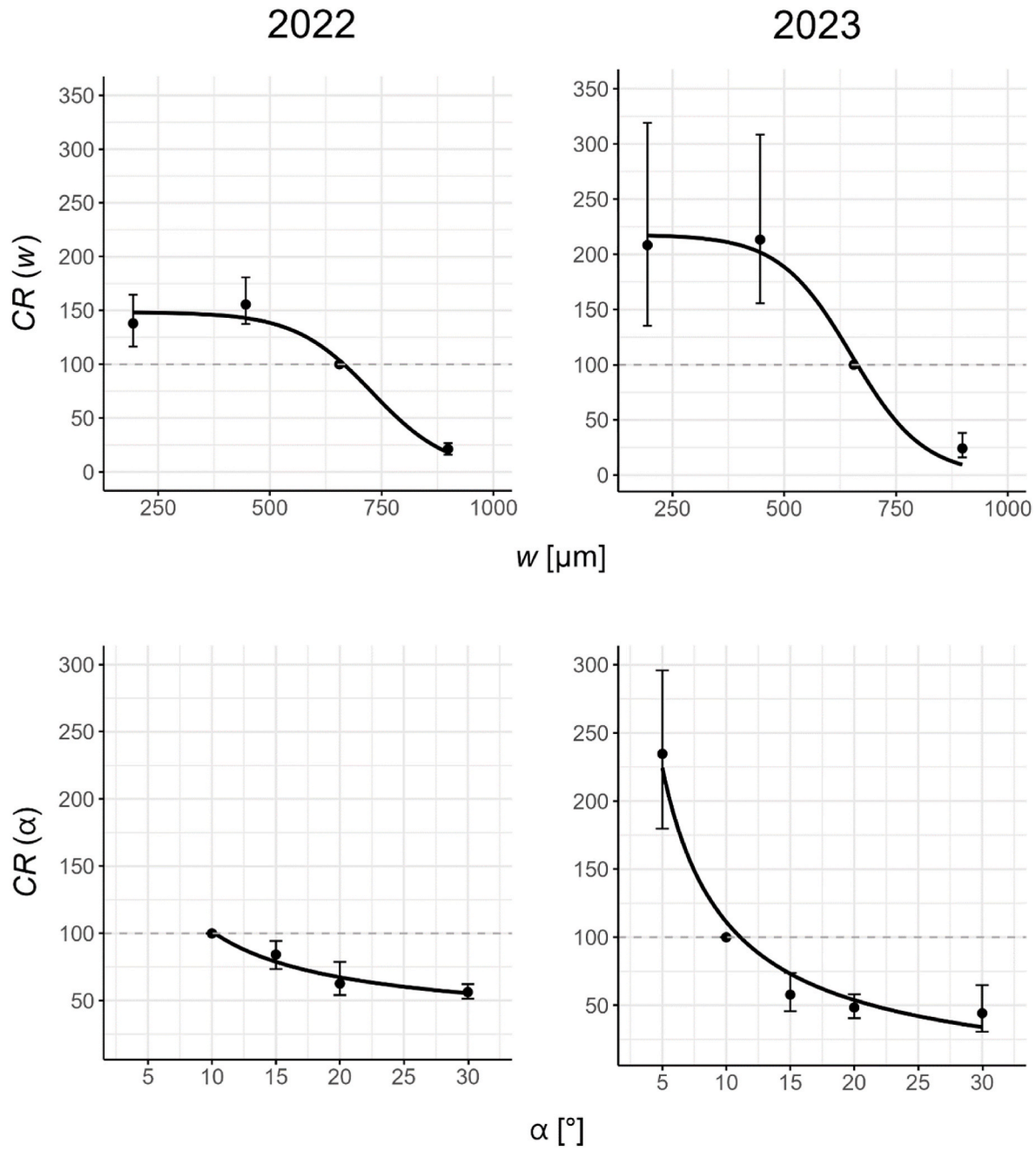


**Fig. 10.** Catch ratio (*CR*) versus mesh size (top) and versus taper angle (bottom) for both years. Error bars represents 95% CIs for the experimental ratios.

Ideally, trade-off functions that simultaneously considered both mesh size and taper angle would be preferred. However, to establish such a model required that both the flume tank and fishing trials involved net designs where the two design parameters (mesh size and taper angle) were varied independent of each other in an experimental matrix design. Specifically, ideally a full design matrix covering all combinations of mesh size and taper angle would mean testing in total of 20 (4 × 5) nets. However, the practical limitations meant we could only test a limited number of combinations in our study. Recognizing these experimental constraints, we chose to quantify the effect of the two parameters independent while keeping the other fixed at a value relevant for use in commercial zooplankton trawls. However, our approach enables us to provide valuable insights on the effect of both mesh size and taper angle when designing commercial zooplankton trawls.

Based on our catch efficiency trade-off functions, we recommend using mesh size around 500 µm, with a solidity ratio below 0.6, and a low taper angle, preferable 5°, as they provided the best trade-offs between catch and drag performances (Fig. 11). The catch ratio functions showed that there was not much improvement in catch performance with mesh sizes below 500 µm (Fig. 10). When the mesh reached a certain small size with a given solidity, it retained all sizes of the *Calanus* sp. Therefore, further decreasing the mesh size while maintaining the same solidity would not result in increased catches. On the other hand, if mesh size is increased too much the entire catch of *Calanus* sp. will be lost. From Fig. 10 it is seen that our 1000 µm net is lost about 75% of what was caught in the 750 µm net. According to Grimaldo et al. (2023) the nets with the highest filtration efficiency were 500 and 750 µm. This is in accordance with our results which show that the highest catch efficiency was achieved with the 500 µm net.

However, this scenario was speculative and requires that the nets are size selective for *Calanus* sp. Therefore, quantifying the effect of mesh size on size selection of *Calanus* sp. is needed for further development of

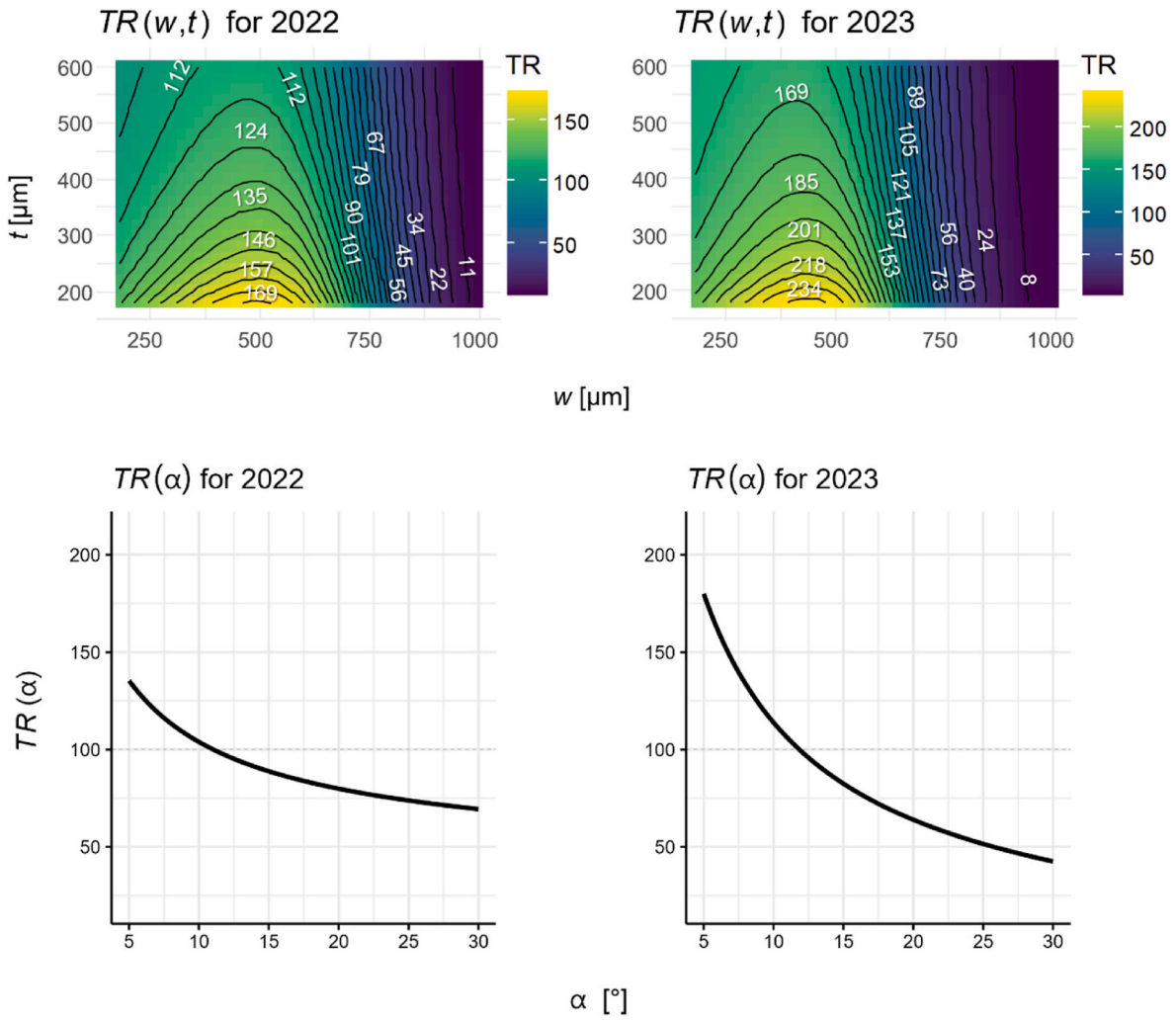


**Fig. 11.** Trade-off (*TR*) curves for each mesh size (*w*) and taper angle ($\alpha$) for both years.

trawls targeting *Calanus* sp. Commercial harvesting of *Calanus* sp. should ideally target large individuals (stages CIV–V) that are rich in oil while releasing small individuals (naupliar stages N1–N6) that are poor in oil reserves (Tande, 1991; Lee et al., 2006). An adjustment of mesh size to match retention of oil-rich individuals would reduce the total drag of the trawls. Skjoldal et al. (2013) previously showed a loss of zooplankton like *Calanus* sp. in different mesh sizes (333 µm compared to 180 µm) via significant escapement and extrusion effects, which indicated the need for further research of the impact of mesh size on *Calanus* sp. size selection. However, such information is limited in the scientific literature and therefore the effect of mesh has yet to be quantified. This process will require application of a size selectivity analysis (Wileman et al., 1996) of small-sized species such as *Calanus* sp. To the best of our knowledge, such a methodology has not yet been developed or at least has not been applied to net catches of *Calanus* sp. Therefore, future studies should assess the effects of further adjustments of mesh size of the nets for targeting the largest sizes with the highest oil content of *Calanus* sp.

The lowest taper angle tested provided the best trade-off between catch and drag performance (Fig. 11), even though drag ratio increased with the lower taper angle (Fig. 8). This was explained by an increase in catch ratio with lower taper angle (Fig. 10) to an extent that more than compensated for the increase in drag. That lower taper angle leads to higher catch efficiency can potentially be explained by the size selection, as the square meshes projected area will appear more rectangular with shorter bar-length in one direction. The meshes will therefore have a smaller opening area for *Calanus* sp. to pass through in the towing direction than if they were perpendicular to the meshes, and this would mean that lower taper angle the ability to retain smaller *Calanus* sp. This mechanism has been used to explain size selection for other bigger-sized species in other fisheries (Jacques et al., 2019; Cuende et al., 2020; Grimaldo et al., 2022).

A practical aspect that highlights the importance of choosing correct mesh size and taper angle is the issue of clogging. Clogging of nets and the consequent reduction of catch efficiency is an important problem that must be addressed to sustain filtration efficiency over longer (>2 h) hauls. In commercial operations, *Calanus* sp. trawls are towed for up to 8–10 h, which may have consequences for the energy and catch efficiency of the gear. To address this problem, commercial vessels have developed a method to wash the *Calanus* sp. trawls as they are pulled on board. However, it is unknown how clogging affects (reduces) catch efficiency and increases the total drag of the trawls. Our study was not designed to assess the effect of clogging of nets on catch efficiency, but we were aware of this potential effect on our study and tried to minimize it. Therefore, to reduce the potential effect of net clogging, the nets were washed after every haul to remove organic material in the nets. Future studies could investigate in the effects of net clogging on catch efficiency and overall gear performance, including potential solutions to address this problem.

Finally, our results are obtained under specific conditions, such as specific water flow and depths, therefore, some caution needs to be taken when extrapolating results to other conditions. However, to

overcome such limitations most of our results are provided as ratio-based values between performance of the designs tested under identical varying conditions. Such ratio-based results are much more robust to extrapolation than absolute values which cannot be extrapolated. The ratio-based technique we have used in this study is one of the main strengths of our study and therefore we believe that our results are of general value.

## CRediT authorship contribution statement

**Enis N. Kostak:** Writing – original draft, Visualization, Validation, Resources, Methodology, Investigation, Formal analysis, Data curation. **Eduardo Grimaldo:** Writing – original draft, Supervision, Project administration, Investigation, Funding acquisition, Data curation, Conceptualization. **Jesse Brinkhof:** Writing – original draft, Supervision, Investigation, Data curation. **Bent Herrmann:** Writing – original draft, Supervision, Methodology, Investigation, Formal analysis, Conceptualization.

## Declaration of competing interest

The authors declare that they have no known competing financial interests or personal relationships that could have appeared to influence the work reported in this paper.

## Data availability

Data will be made available on request.

## Acknowledgments

This study was funded by a SFI Harvest research project (Grant no: 309661, from the Research Council of Norway 2020–2028). We thank to the crew of R/V Helmer Hanssen and the staff at the North Sea A/S flume tank for assistance during the data collection. We also thank Waranya Wataniyakun, Kristine Cerbule, Amanda Schadeberg, and Ilmar Brinkhof for their help during the sea trials.

## Appendix A. Supplementary data

Supplementary data to this article can be found online at https://doi.org/10.1016/j.oceaneng.2024.118097.

## Appendix

This appendix derives an equation for how netting solidity depends on the netting parameters mesh size ($w$) and twine thickness ($t$) (Fig. A1).

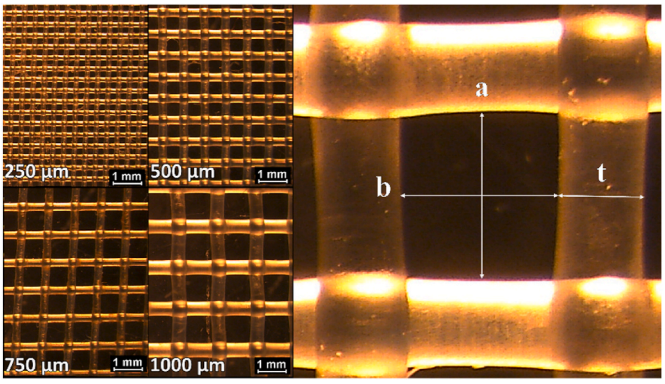


**Fig. A1.** Images of the net samples taken with the Leica microscope (left). Measured points from the mesh and their positions in the image (right).

It is an assumption that nettings can be approximated as square mesh netting. $w$ is approximated by:

$$w = \frac{a+b}{2} \tag{A1}$$

If we assume that the meshes are approximately square-shaped, we have:

$$\begin{aligned} a &\cong w \\ b &\cong w \end{aligned} \tag{A2}$$

With the netting solidity $s$ being the ratio of the area covered with material to the total area of the netting, simple geometry based on Fig. A1 leads to:

$$s = \frac{t \times (t+b) + t \times a}{t \times (t+b) + t \times a + a \times b} = \frac{t \times (t+a+b)}{t \times (t+a+b) + a \times b} \tag{A3}$$

Inserting (A2) in (A3) leads to:

$$s \cong \frac{t \times (t+2 \times w)}{t \times (t+2 \times w) + w^2} \tag{A4}$$

## References


Aarflot, J.M., Skjoldal, H.R., Dalpadado, P., Skern-Mauritzen, M., 2018. Contribution of Calanus species to the mesozooplankton biomass in the Barents Sea. ICES J. Mar. Sci. 75 (7), 2342–2354. https://doi.org/10.1093/icesjms/fsx221.

Akaike, H., 1974. A new look at the statistical model identification. IEEE Trans. Automat. Control 19 (6), 716–723. https://doi.org/10.1109/TAC.1974.1100705.

Barnes, H., Tranter, D.J., 1965. A statistical examination of the catches, numbers, and biomass taken by three commonly used plankton nets. Mar. Freshw. Res. 16 (3), 293–306.

Breddermann, K., 2017. Filtration Performance of Plankton Nets Used to Catch Micro- and Mesozooplankton, vol. 12. Rostocker Meerestechnische Reihe. ISBN-103844054057.

Broms, C., Strand, E., Utne, K.R., Hjøllo, S., Sundby, S., Melle, W., 2016. Vitenskapelig Bakgrunnsmateriale for Forvaltningsplan for Raudåte.

Cerbule, K., Grimsmo, L., Herrmann, B., Grimaldo, E., 2023. Increasing sustainability in food production by using alternative bait in snow crab (Chionoecetes opilio) fishery in the Barents sea. Heliyon 9 (3), e13820. https://doi.org/10.1016/j.heliyon.2023.e13820.

Cuende, E., Arregi, L., Herrmann, B., Sistiaga, M., Aboitiz, X., 2020. Prediction of square mesh panel and codend size selectivity of blue whiting based on fish morphology. ICES J. Mar. Sci. 77 (7–8), 2857–2869. https://doi.org/10.1093/icesjms/fsaa156.

Efron, B., 1982. The jackknife, the bootstrap and other resampling plans. SIAM Monograph No. 38, CBSM-NSF.

Enerhaug, B., 2005. Flow through fine-meshed pelagic trawls. In: Lee, C.-W. (Ed.), Contributions on the Theory of Fishing Gears and Related Marine Systems, DEMaT 2005, vol. 4. Busan, Korea, pp. 153–164.

Evans, M., Sell, D., 1985. Mesh size and collection characteristics of 50-cm diameter conical plankton nets. Hydrobiologia 122, 97–104. https://doi.org/10.1007/BF00032095.

Falk-Petersen, S., Gatten, R.R., Sargent, J.R., Hopkins, C.C.E., 1981. Ecological investigations on the zooplankton community in Balsfjorden, Northern Norway: seasonal changes in the lipid class composition of Meganyctiphanes norvegica (M. Sars), Thysanoessa raschii (M. Sars), and T. inermis (Krøyer). J. Exp. Mar. Biol. Ecol. 54 (3), 209–224. https://doi.org/10.1016/0022-0981(81)90065-4.

Frandsen, R.P., Herrmann, B., Madsen, N., Krag, L.A., 2011. Development of a codend concept to improve size selectivity of Nephrops (Nephrops norvegicus) in a multi-species fishery. Fish. Res. 111 (1–2), 116–126. https://doi.org/10.1016/j.fishres.2011.07.003.

Fridman, A.L., 1986. Calculations for fishing gears designs. FAO Fishing Manuals. FAO Fishing New Books Ltd., Farnham, UK 69, 71.

Gjøsund, S.H., Enerhaug, B., 2010. Flow through nets and trawls of low porosity. Ocean Eng. 37 (4), 345–354. https://doi.org/10.1016/j.oceaneng.2010.01.003.

Grimaldo, E., Gjøsund, S.H., 2012. Commercial exploitation of zooplankton in the Norwegian Sea. In: Ali, M. (Ed.), The Functioning of Ecosystems. InTech, pp. 213–228. ISBN-978-953-51-0573-2.

Grimaldo, E., Herrmann, B., Brčić, J., Cerbule, K., Brinkhof, J., Grimsmo, L., Jacques, N., 2022. Prediction of potential net panel selectivity in mesopelagic trawls. Ocean Eng. 260, 111964 https://doi.org/10.1016/j.oceaneng.2022.111964.

Grimaldo, E., Herrmann, B., Kostak, E.N., Brinkhof, J., 2023. Understanding the effect of design parameters on the filtration efficiency of trawls intended for commercial harvesting of zooplankton. Ocean Eng. 288, 116141 https://doi.org/10.1016/j.oceaneng.2023.116141.

Hernroth, L., 1987. Sampling and filtration efficiency of two commonly used plankton nets. A comparative study of the Nansen net and the UNESCO WP 2 net. J. Plankton Res. 9 (4), 719–728.

Herrmann, B., Krag, L.A., Frandsen, R.P., Madsen, N., Lundgren, B., Stæhr, K.J., 2009. Prediction of selectivity from morphological conditions: methodology and a case study on cod (Gadus morhua). Fish. Res. 97 (1–2), 59–71. https://doi.org/10.1016/j.fishres.2009.01.002.

Herrmann, B., Sistiaga, M.B., Nielsen, K.N., Larsen, R.B., 2012. Understanding the size selectivity of redfish (Sebastes spp.) in North Atlantic trawl codends. https://doi.org/10.2960/J.v44.m680.

Herrmann, B., Cerbule, K., Brčić, J., Grimaldo, E., Geoffroy, M., Daase, M., Berge, J., 2022. Accounting for uncertainties in biodiversity estimations: a new methodology and its application to the mesopelagic sound scattering layer of the high Arctic. Front. Ecol. Evol. 10, 775759 https://doi.org/10.3389/fevo.2022.775759.

Jacques, N., Herrmann, B., Larsen, R.B., Sistiaga, M., Brčić, J., Gökçe, G., Brinkhof, J., 2019. Can a large-mesh sieve panel replace or supplement the Nordmøre grid for bycatch mitigation in the northeast Atlantic deep-water shrimp fishery? Fish. Res. 219, 105324 https://doi.org/10.1016/j.fishres.2019.105324.

Lee, R.F., Hagen, W., Kattner, G., 2006. Lipid storage in marine zooplankton. Mar. Ecol. Prog. Ser. 307, 273–306. https://doi.org/10.3354/meps307273.

McBride, M.M., Dalpadado, P., Drinkwater, K.F., Godø, O.R., Hobday, A.J., Hollowed, A. B., Loeng, H., 2014. Krill, climate, and contrasting future scenarios for Arctic and Antarctic fisheries. ICES J. Mar. Sci. 71 (7), 1934–1955. https://doi.org/10.1093/icesjms/fsu002.

Norwegian Directorate of Fisheries, 2022. Norwegian Directorate of Fisheries Economic and biological figures from Norwegian fisheries 2022. Available at: https://www.fiskeridir.no/English/Fisheries/Statistics/Economic-and-biological-key-figures.

Skjoldal, H.R., 2004. The Norwegian Sea Ecosystem. Tapir Academic Press, p. 559.

Skjoldal, H.R., Wiebe, P.H., Postel, L., Knutsen, T., Kaartvedt, S., Sameoto, D.D., 2013. Intercomparison of zooplankton (net) sampling systems: results from the ICES/GLOBEC sea-going workshop. Prog. Oceanogr. 108, 1–42. https://doi.org/10.1016/j.pocean.2012.10.006.

Tande, K.S., 1991. Calanus in North Norwegian fjords and in the barents sea. Polar Res. 10 (2), 389–408. https://doi.org/10.1111/j.1751-8369.1991.tb00661.x.

Tosetto, E.G., Neumann-Leitão, S., Júnior, M.N., 2019. Sampling planktonic cnidarians with paired nets: implications of mesh size on community structure and abundance. Estuarine. Coast Shelf Sci. 220, 48–53. https://doi.org/10.1016/j.ecss.2019.02.031.

Tranter, D., 1967. A formula for the filtration coefficient of a plankton net. Mar. Freshw. Res. 18, 113–122. https://doi.org/10.1071/MF9670113.

Tranter, D., Heron, A., 1967. Experiments on filtration in plankton nets. Mar. Freshw. Res. 18, 89–112. https://doi.org/10.1071/MF9670089.

Wileman, D.A., Ferro, R.S.T., Fonteyne, R., Millar, R.B., 1996. Manual of methods of measuring the selectivity of towed fishing gears. ICES Coop. Res. Rep. https://doi.org/10.17895/ices.pub.4628.

Xiping, L., Yehui, T., Yonghong, L., 2013. Comparison of capture efficiency for zooplankton in the northern South China Sea, using two plankton mesh sizes. J.Trop. Oceanogr. 32 (3), 33–39.

Zhou, C., Xu, L., Hu, F., Qu, X., 2015. Hydrodynamic characteristics of knotless nylon netting normal to free stream and effect of inclination. Ocean Eng. 110, 89–97. https://doi.org/10.1016/j.oceaneng.2015.09.043.